Visible emission from AlN doped with Eu and Tb ions

W. M. Jadwisienczak and H. J. Lozykowski[a)]
School of Electrical Engineering & Computer Science, Ohio University, Athens, Ohio 45701

I. Berishev and A. Bensaoula
Nitride Materials and Devices Laboratory, University of Houston, Houston, Texas 77204

I. G. Brown
Lawrence Berkeley National Laboratory, University of California, Berkeley, California 94720

(Received 2 January 2001; accepted for publication 30 January 2001)

We report the observation of visible cathodoluminescence (CL) from AlN thin films grown on sapphire (0001) substrate by molecular beam epitaxy and doped by implantation with Eu^{3+} and Tb^{3+} ions. The strongest rare earth (RE) CL was observed from samples annealed at 1100 °C for 0.5 h in N_2 ambient. The sharp characteristic emission lines corresponding to Eu^{3+} and Tb^{3+} intra-$4f^n$ shell transitions are resolved in the spectral range from 350 to 900 nm. The CL spectra were recorded over 1–16 keV electron energy in the temperature range of 8–330 K. The depth resolved CL spectral analysis gives the luminescence surface a dead layer thickness of ~16 nm for implanted AlN samples. We observed several different recombination centers luminescing in the 286–480 nm spectral region due to the presence of structural defects and oxygen impurities. The time resolved spectra and the CL kinetics were studied. The decay times for $^5D_0 \rightarrow {}^7F_2$ (Eu^{3+}), $^5D_3 \rightarrow {}^7F_5$ (Tb^{3+}), and $^5D_4 \rightarrow {}^7F_6$ (Tb^{3+}) transitions at 300 K are ~0.4, ~0.9, and ~0.4 ms, respectively. We also discuss possible excitation mechanisms of RE ions in AlN. © *2001 American Institute of Physics.* [DOI: 10.1063/1.1357467]

I. INTRODUCTION

There has been increasing interest in rare earth (RE) doped III-nitride semiconductors due to their potential applications in photonics systems. The AlN and AlGaN are interesting hosts for RE ions because of light emitting and waveguide devices. The advantage of AlN waveguides with a refractive index $n=2.1-2.2$ for single crystal epitaxial films (1.9–2.1 for polycrystalline films, 1.8–1.9 for amorphous) cladded with Al_2O_3 ($n=1.64$) or SiO_2 ($n=1.45$) is that the high index difference between the core and cladding results in high confinement of optical modes in the waveguide. This ensures efficient amplification and pumping, as well as allowing small waveguide bending radii for device applications. Furthermore, its thermal and chemical stabilities make it attractive for the generation, guiding, and switching of light. The potential of waveguides, fiber amplifiers, and narrow-band lasers in optical communication systems, which stimulated the initial development of this technology, was confirmed by the spectacular emergence of erbium doped fiber amplifiers.[1,2] Recently infrared and visible emissions from Er doped crystalline AlN,[3,4] Er, and Tb doped amorphous AlN,[5,6] as well as from AlGaN/GaN superlattice implanted with Eu,[7] were reported.

II. SAMPLES AND MEASUREMENT

In this article we focus on measurements for visible emissions from single crystal AlN thin films doped by implantation with Eu^{3+} and Tb^{3+}. The AlN samples used in this study were grown on sapphire (0001) wafers by plasma source molecular beam epitaxy in a custom designed ultra-high vacuum chamber with a base pressure lower than 1×10^{-9} Torr. The growth chamber has, among other sources, an EPI Uni-bulb radio frequency (rf) plasma source for delivery of excited nitrogen and a 35 cm^3 cold lip effusion cell for Al.[8] Prior to growth, the substrate was degreased by boiling in organic solvents, etched for 1 min in a solution of $3{:}H_2SO_4{-}1{:}H_2O_2{-}1{:}H_2O$, rinsed in de-ionized water, and dried in nitrogen. In order to ensure homogeneous radiative heating of the sapphire in vacuum, a 0.2-mm-thick Mo layer was deposited on the backside of the wafer by e-beam evaporation. The sapphire wafer was then annealed in a vacuum to 800 °C. This step was followed by surface nitridation of the wafer which was carried out for 1 h under the following conditions: sample temperature of 750 °C as measured by a pyrometer, a rf power of 400 W, and a nitrogen flow of 1 sccm. The growth of the AlN epilayer was conducted at a sample temperature of 750 °C using an Al beam equivalent pressure of 7.1×10^{-7} and the same nitrogen source setting as described above. This Al flux corresponds to a near-to unity ratio between the group III and V fluxes.

AlN films (~1 μm thick) were doped by implantation with Eu and Tb ions at room temperature. Each RE ion was implanted at four energies (150, 75, 38, and 17 keV) at doses chosen to give an approximately flat implant concentration depth profile in the AlN layer. The implanting ion beam was inclined at 7° to the normal of the AlN epilayer to prevent channeling. A computer simulation of the depth profiles (Pearson's distribution) indicates penetration depths for implanted ions approximately at the same range (~45 nm) with

a)Electronic mail: lozykows@bobcat.ent.ohiou.edu

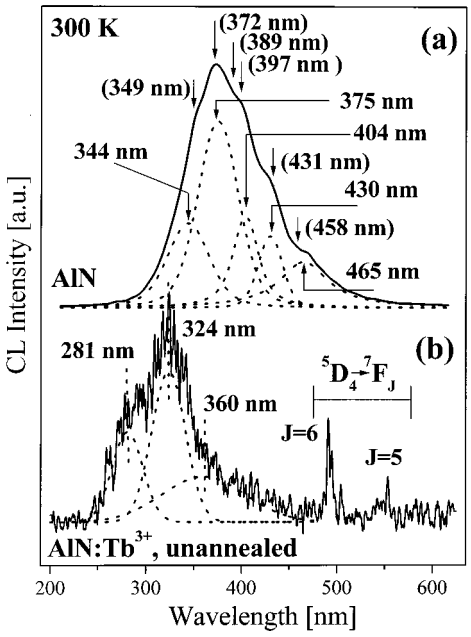

FIG. 1. CL emission from an unannealed reference AlN sample (a) excited by electron beam (9 keV, 1 mA/cm^2) and measured at 300 K (solid line) together with peaks obtained from deconvolution to Voigt bands (dotted lines). Numbers in parentheses indicate the bands' peak positions reported by Morita (Ref. 9a) and attributed to nitrogen vacancies or interstitial Al (349 and 372 nm), and to oxygen impurity defects (431 and 458 nm) respectively. CL emission from an unannealed Tb doped AlN sample (b) excited by electron beam (9 keV, 1 mA/cm^2) and measured at 300 K (solid line) together with bands at 281, 324, and 360 nm obtained from deconvolution to Voigt bands (dotted lines).

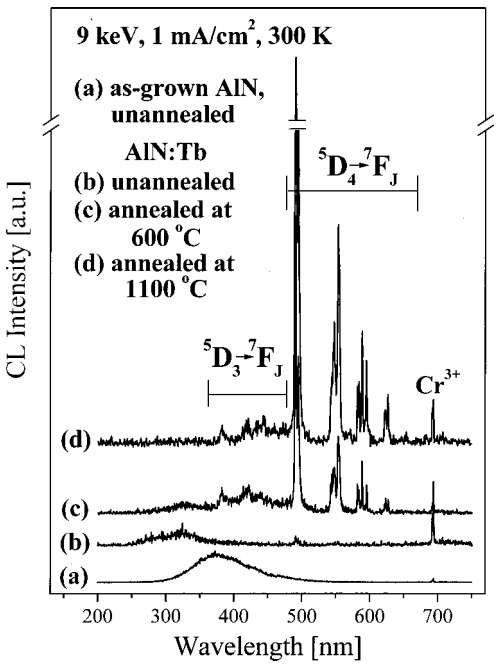

FIG. 2. Evolution of CL Tb^{3+} ions emission as a function of annealing temperature, recorded at 300 K under electron beam parameters described in the figure. Spectrum (a) is for unannealed reference AlN sample, spectrum (b) is for unannealed Tb implanted AlN sample, spectra (c) and (d) are for AlN:Tb samples annealed for 30 min in N_2 ambient at 600 °C (c), 1100 °C (d), respectively. All spectra were normalized with respect to the strongest peak of curve (d) at 492 nm and artificially shifted for clarity.

the peak concentrations for: Eu^{3+} 3.9×10^{19} At/cm^3 and Tb^{3+} 4.01×10^{19} At/cm^3, respectively. To optically activate incorporated impurities and remove ion implantation-induced damage, the implanted AlN samples were subjected to postimplantation isochronal thermal annealing treatments (duration 30 min) in temperatures from 500 to 1100 °C in a tube furnace under a flow of N_2 at atmospheric pressure. Subsequently spectroscopic studies were conducted including cathodoluminescence (CL) as a function of temperature depth resolved CL spectra, the CL time resolved (CL TRS), and CL kinetics using experimental setup and apparatus described elsewhere.[6]

III. RESULTS AND DISCUSSION

The CL spectra of undoped and Tb doped AlN samples measured at 300 K in the spectral range from 200 to 620 nm are shown in Fig. 1. The spectrum (a) is the CL emission from an unannealed reference AlN sample which contains a broad modulated band centered at 375 nm. The weak modulation of the broadband can be attributed to an interference in the microcavity formed by the AlN-air and AlN-sapphire substrate interface. However, some of the bands obtained from deconvolution (to Voigt bands) of this broad modulated spectrum have peak positions matching well with bands and humps observed by Morita and others.[6,9(a)–(c)] They were observed at 349, 372, 389, 397, 431, and 458 nm and assigned as follows: the first two to nitrogen vacancies or interstitial Al, and the last two bands were attributed to oxygen impurity defects induced by the increase in oxygen concentration. Oxygen is a very common impurity in AlN and its luminescence has been reported in a wide spectral range from 295 to 443 nm.[9(b)]

The evolution of the AlN:Tb^{3+} CL emission spectra as a function of annealing temperature measured at 300 K under identical excitation conditions are shown in Fig. 2. The spectrum (a) in Fig. 2 is the CL emission of an AlN as grown unannealed reference sample. The weak line at 694 nm is the Cr^{3+} emission line originating from the sapphire substrate.[7] Spectrum (b) is for the AlN:Tb unannealed sample, spectra (c) and (d) are for samples annealed at 600 and 1100 °C, respectively. It can be seen that only very weak emissions from a terbium ion are detected after implantation. The characteristic $4f$ emission for all investigated RE ions in an AlN host start to appear at annealing temperatures about 600 °C and increase as a function of the annealing temperature. The strongest emission from RE^{3+} ions was observed for samples annealed at 1100 °C and is about 35 and 25 times stronger (for Tb^{3+} and Eu^{3+}, respectively) than for implanted and unannealed samples. We have reported a similar observation for amorphous AlN:Tb.[6] CL spectra of AlN samples doped with Eu and Tb annealed at 1100 °C recorded at 7 and 300 K are shown in Figs. 3(a) and 3(b). The excitation parameters are described in the figures together with the assignment for most of the RE^{3+} transitions based upon their correspondence with the wavelength of luminescence lines of RE^{3+} in other hosts.[10] The CL emission of Eu^{3+} ($4f^6$) implanted into AlN measured at 300 K in Fig. 3(a) exhibits several groups of emission lines linked to transitions from $^5D_1$ and $^5D_0$ to

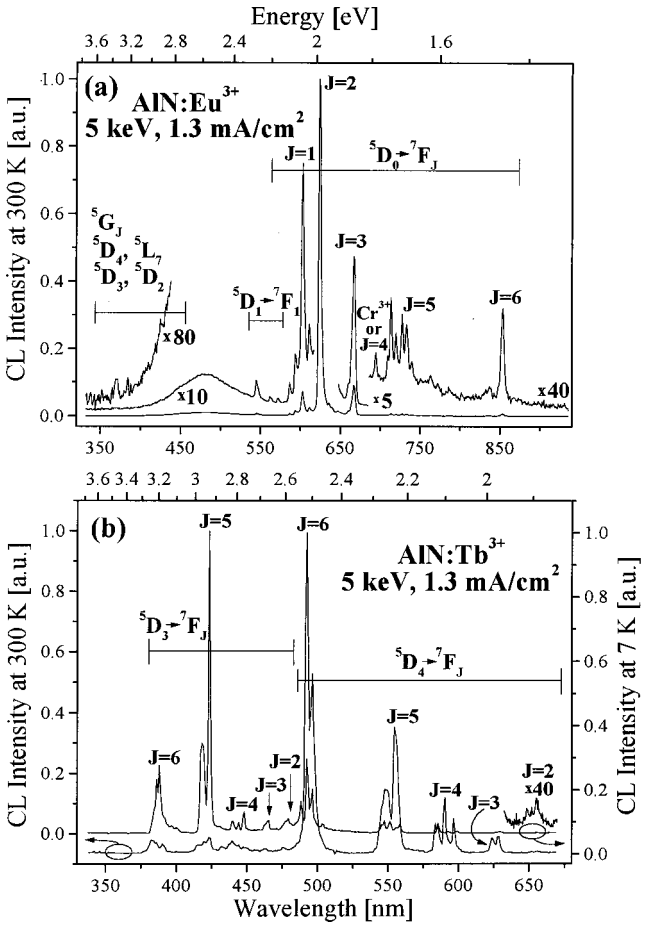

FIG. 3. CL spectra of AlN doped with Eu^{3+} (a) and Tb^{3+} (b) recorded at 7 K (right scale) and 300 K (left scales) excited by electron beam with energy 5 keV and current 1 mA/cm^2 measured under identical excitation conditions.

levels of the ^7F_J ground terms, and the much weaker emissions from electronic states ^5G_J, $^5L_7$, $^5D_4$, $^5D_3$, and $^5D_2$. We also observed the broadband at 475 nm due to the host emission. The CL spectra of AlN doped with Tb^{3+} ($4f^8$) recorded at 7 K (upper spectrum) and 300 K (a lower spectrum) are shown in Fig. 3(b). The sharp line structures arise from $^5D_4$ and $^5D_3$ emissions to the ^7F_J multiplets. The $^5D_3 \rightarrow {}^7F_{2,1,0}$ transitions are masked by the more intense $^5D_4 \rightarrow {}^7F_6$ emission that occurs at a similar energy, and could not be clearly observed.

In order to determine the CL depth resolved spectra from Eu and Tb doped AlN samples we recorded emission spectra under a constant excitation power of $P_b = 4.26\,\mathrm{W/cm^2}$ with electron acceleration voltage varying from 0.5 to 16 kV. The CL experimental data were obtained for the incident electron beam at an angle 45° to the normal. The electron penetration depths were obtained using three methods, the Norris (R_N) scaling technique,[11(a)] the Kanaya–Okayama model (R_{KO}),[11(b)] and Monte Carlo (MC) simulations (R_{MC}).[11(c)–(e)] The penetration range R_N was calculated by scaling normal incidence data for Si according to the density ratio of Si and AlN, the R_{KO} is calculated using the Kanaya–Okayama equation, and the R_{MC} was obtained from the MC simulations. The MC simulations were performed for incident beam angles of 0° and 45° to the normal. At each electron beam energy, 10^5 electron trajectories were simulated to obtain satisfactory statistical accuracy. The MC simulations accurately calculate the total electron energy loss profiles (depth and lateral) of primary electron interactions in materials. When the incident angle is 45° to the normal, the interaction volume becomes asymmetric about the beam axis and the depth dimension of the envelope containing a given fraction of the trajectories falls. As an approximation, the R_{MC} and R_{KO} penetration depths for tilted sample are given by $R(\alpha) = R_\perp \mathrm{Cos}(\alpha)$, where $R_\perp$ is the penetration depth at normal incident, and α is the incident angle. Table I summarize the maximum penetration depth obtained from the above methods using a density of 2.33 g/cm^3 for Si and 3.26 g/cm^3 for AlN.

TABLE I. The electron penetration depth (R) as a function of energy calculated at a normal and 45° incidence for AlN. The R_N is calculated by scaling normal incidence data for Si according to the density ratio of Si and AlN [Ref. 11(a)], the R_{KO} is calculated from Kanaya–Okayama model [Ref. 11(b)], and the R_{MC} is obtained from the Monte Carlo simulation [Refs. 11(c)–(e)] (10^5 electron trajectories at each electron beam energy).

Electron energy [keV]	Incident angle	R_N[11(a)] [μm]	R_{KO}[11(b)] [μm]	R_{MC}[11(c)–(e)] [μm]
1.6	0°	0.033	0.053	0.021
	45°		0.038	0.016
3.0	0°	0.096	0.15	0.058
	45°		0.11	0.046
6.0	0°	0.32	0.48	0.19
	45°		0.34	0.15
9.0	0°	0.64	0.95	0.38
	45°		0.67	0.30
12.0	0°	1.05	1.53	0.63
	45°		1.08	0.50
16.0	0°	1.72	2.48	1.01
	45°		1.75	0.81

The R_{KO} and R_{MC} penetration depths calculated at incident angle 45° are plotted in Fig. 4 showing that the penetration depth R_{KO} is bigger than R_{MC}. The MC simulations provide more reliable results in good agreement for a depth

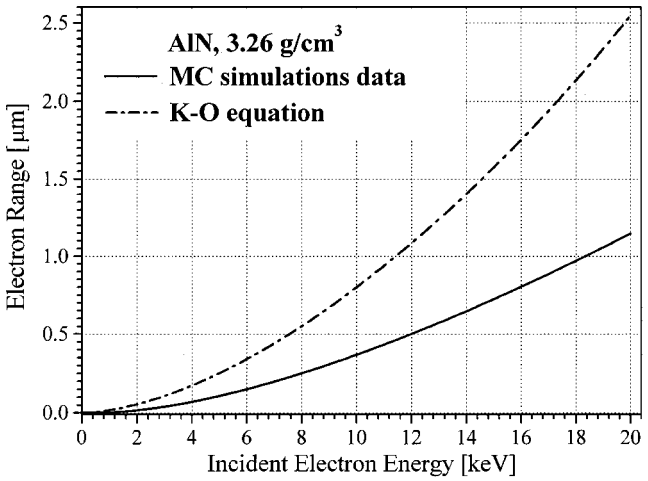

FIG. 4. The electron beam range as a function of the incident electron energy calculated for AlN epilayer using the (a) Monte Carlo simulations and (b) Kanaya–Okayama equation, for the incident beam angle 45° to the normal.

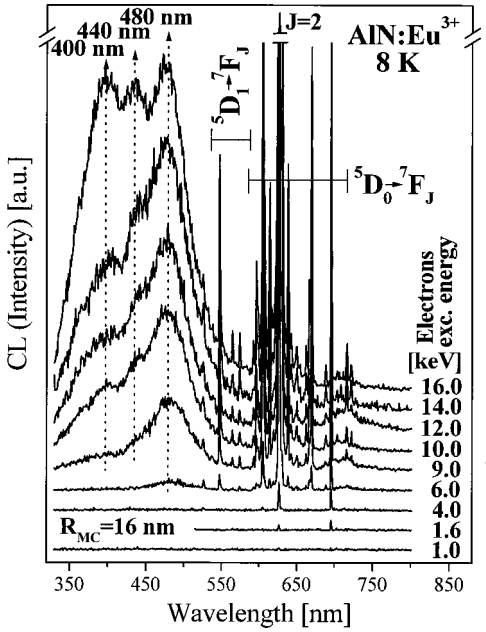

FIG. 5. Depth resolved CL spectra of AlN:Eu^{3+} measured at 8 K and constant beam power excitation conditions (4.2 W/cm^2) artificially shifted up for clarity. The emission line $^5D_0 \rightarrow {}^7F_2$ recorded at 16 keV is 25 times stronger than the band at 480 nm (figure shows only ~6% total intensity of this transition).

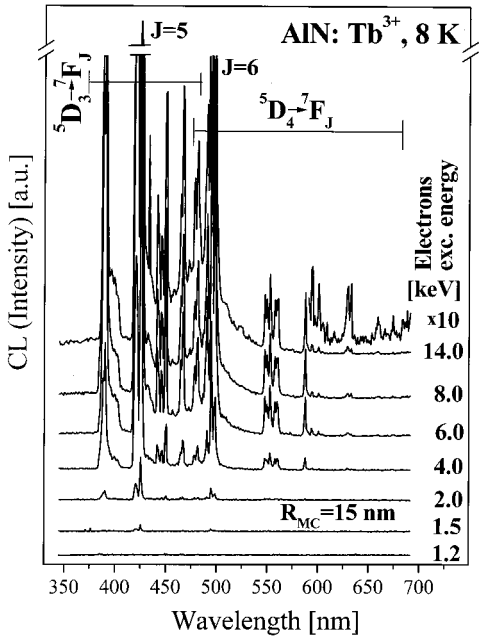

FIG. 6. Depth resolved CL spectra of AlN:Tb^{3+} measured at 8 K and constant beam power excitation conditions (4.2 W/cm^2) artificially shifted up for clarity. The emission line $^5D_3 \rightarrow {}^7F_5$ recorded at 14 keV is 50 times stronger than the band at 480 nm (figure shows only ~3% total intensity of this transition).

profile and for absolute values of the energy dissipation between the experimental and the calculation data.[12]

The depth resolved CL spectra measured at 8 K for AlN:Eu and for AlN:Tb are shown in Figs. 5 and 6, respectively. The Eu^{3+} and Tb^{3+} ion emissions are detected beginning at approximately 1.5 and 1.6 keV which corresponds to an electron penetration depth $R_{MC} \sim 15$ nm (Tb) and $R_{MC} \sim 16$ nm (Eu), respectively. The emission spectra up to 3 keV contain only characteristic $4f$-$4f$ sharp lines attributed to Eu^{3+} and Tb^{3+} ions without any AlN host broadband emission background. At an electron acceleration voltage above ~4 kV ($R_{MC}=75$ nm), a broadband centered at 480 nm starts to appear, and grows with increasing beam energy, which is seen for AlN doped with Eu samples in Fig. 5. At acceleration voltages higher than 9 kV ($R_{MC}=300$ nm), two new bands emerge at 400 and 440 nm and overlap with the existing band at ~480 nm. With still higher acceleration voltage the ~480 nm emission band intensity increases while the two shorter wavelength bands at 400 and 440 nm increase faster and become equal with the band peaking at ~480 nm at acceleration voltage 16 kV ($R_{MC}=810$ nm). Note that the intensities of Eu^{3+} transitions from $^5D_0$ to $^7F_{1,2,3}$ levels are much stronger than the broadband at 480 nm. At electron excitation energy of 16 keV the emission line $^5D_0 \rightarrow {}^7F_2$ is 25 times stronger than the band at 480 nm (Fig. 5 shows only 6% total intensity of transition $^5D_0 \rightarrow {}^7F_2$) A closer look at Fig. 1 (upper spectrum) reveals that their positions are close to the bands position obtained from the deconvolution analyses done for the reference AlN sample. For Tb doped AlN samples (Fig. 6), the emission is dominated by terbium line emission in the blue and green spectral region, and the existence of the host wideband background is barely noticeable. The dominant $^5D_3 \rightarrow {}^7F_5$ transition is about 50 times stronger than the broadband at ~480 nm which start to appear at ~4 keV. To separate the Tb^{3+} emission from the AlN host band we measured the CL TRS shown in Fig. 7. The spectra were recorded at 9 K using as excitation source a pulsed electron beam with an energy of 9 keV and current density 1 mA/cm^2 for different delay times.

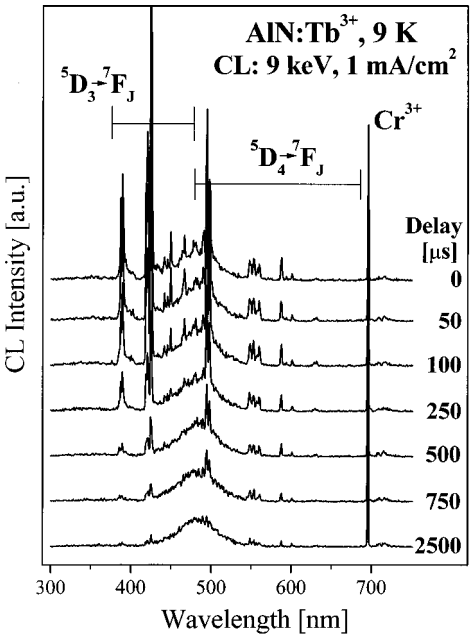

FIG. 7. CL time resolved spectra of AlN:Tb^{3+} recorded at 8 K with pulsed electron beam energy 9 keV and current 1 mA/cm^2. After delay time of 2.5 ms the AlN host emission dominates the spectrum.

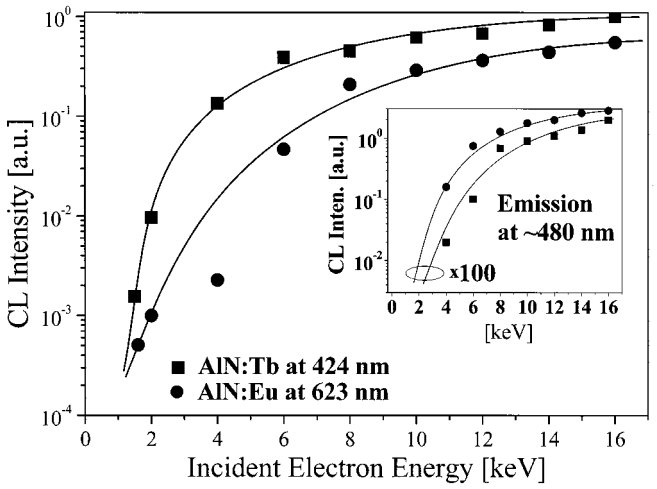

FIG. 8. Variation of CL intensity of selected Tb^{3+} ($^5D_3 \rightarrow {}^7F_5$) (■) at 424 nm and Eu^{3+} ($^5D_0 \rightarrow {}^7F_2$) (●) at 623 nm emission lines as a function of incident electron excitation energy. Inset shows the intensity of the host emission monitored at 480 nm vs incident electron excitation energy. All emission peak intensities were normalized to the strongest Tb peak at 424 nm. The solid lines are added as an aid to the eyes.

The CL spectra show transitions which originate in $^5D_3$ and $^5D_4$ levels and terminate in the ^7F manifolds superimposed on a weak broadband peaking at approximately 480 nm. The Tb^{3+} emission line intensity gradually decreases with increased delay time and is clearly seen even for 2.5 ms delays after an excitation electron beam pulse. For the 2.5 ms delay the host emission at ~480 nm and Cr^{3+} line at 694 nm dominate the spectrum (Fig. 7). Furthermore, for the AlN:Tb samples we did not observed broadband emission at ~480 nm as clearly as we did for the reference and Eu doped AlN samples under the same excitation conditions. The position of this band coincides with the band at 480 nm observed for AlN:Eu and AlN reference samples which are shown in Fig. 1(a) and Fig. 5. The CL TRS of AlN doped with Eu (not shown) measured under the same excitation conditions does not exhibit any difference in AlN host emission, but the lines due to Eu^{3+} transitions decay faster and almost vanish for 2.0 ms delays after an excitation electron beam pulse. Variation of the emission intensities for transitions $^5D_0 \rightarrow {}^7F_2(Eu^{3+})$ and $^5D_3 \rightarrow {}^7F_5(Tb^{3+})$ as well as the host band emission as a function of incident electron energy is shown in Fig. 8. We observed that the emission intensity of Tb ions increases faster than the emission intensity of Eu ions in the excitation energy range from 2 to 16 keV, whereas the host band emission at 480 nm gains intensity faster for AlN doped with Eu than for AlN sample doped with Tb (inset of Fig. 8). The host emission band emerges at approximately ~4 keV for Eu^{3+} and Tb^{3+} which correspond to $R_{MC} \sim 75$ nm. In cathodoluminescence the RE ions can be excited via direct impact with hot electrons, as well as by energy transfer processes from the generated electron-hole pairs or by impact excitation (or ionization) involving other impurities (or complex defects) with subsequent energy transfers to RE $4f$ shell electrons. An important issue of the RE ions excitation process is the RE ion-host lattice coupling strength, which is determined by RE ion lattice site location and the local microstructure around the RE ions. The space group symmetry of wurtzite AlN crystal is $C_{6v}^4 - P6_3mc$ and the Al cation occupies the site of point group symmetry C_{3v}. Recently, using the emission channeling technique, the lattice site occupation of light alkalis Li, Na, and In and Sr in AlN were determined as relaxed substitutional Al sites.[13] It is generally accepted that rare earth impurities in III–V semiconductors create isoelectronic traps.[14] On the basis of the above experimental finding and the crystal field calculation for Pr^{3+} in GaN,[15] and discussion presented by Lozykowski,[14] the Al sites are the most probable locations for rare earth ions in AlN. The RE ions in hexagonal AlN occupy relaxed cation sites of C_{3v} symmetry. The outer electron configurations of RE^{3+} ions are the same ($5s^25p^6$). If the RE^{3+} ions replace the element from column III (Al^{3+}, Ga^{3+}) in III-nitride semiconductors that are isovalent concerning outer electrons of RE^{3+} ions, we believe that they create isoelectronic traps in III-nitrides (REI trap). This conclusion is supported by the fact that the atomic covalent radii (ionic RE^{3+}) for all rare earths are greater than the atomic radii of Al and Ga that they are replacing. Pauling's electronegativity X_{RE} of RE elements (1.1–1.25) is smaller than $X_{Ga,\,Al}$Ga(1.81), and Al(1.61) for which it substitutes. Assuming that REI traps are created in AlN we may consider the several possible mechanisms of energy transfer. The first is the energy transfer process from excitons bound to structured isoelectronic centers to core electrons. The second mechanism is the transfer of energy to the core electrons involving the structured isoelectronic trap (or other intermediate state) occupied by electrons (holes) and free holes (electrons) in the valence (conduction) band. A third mechanism is transfer through an inelastic scattering process in which the energy of a free exciton near a REI trap is given to the localized core excited states. If the initial and final states are not resonant, the energy mismatch must be distributed in some way, e.g., by phonon emission or absorption. In C_{3v} crystal symmetry the states with $J=0$, 1, 2, 3, 4, 5, 6, will split into 1(0), 1(1), 1(2), 3(2), 3(3), 3(4), 5(4), single (doubly) degenerated crystal field *LSJ* levels, respectively. The rare earth ions located at a specific crystal site are associated with characteristic optical transitions subject to the selection rules that are governed by the crystal symmetry of the site. Extracting symmetry information of RE^{3+} centers from the sharp lines $4f^n$ luminescence spectrum is difficult. This is because, besides the purely electronic lines, CL spectra contain vibronic and satellite lines, lines due to other site symmetry, and in real crystals, lines due to the splitting of doubly degenerated in pure C_{3v} symmetry crystal field levels.

To get a better insight into the nature of energy migration processes we studied the CL and CL kinetics of investigated RE ion emission lines as a function of temperature. The CL intensity of AlN:Eu strongest lines, attributed to magnetic-dipole $^5D_0 \rightarrow {}^7F_1(602\,\text{nm})$ and electric-dipole $^5D_0 \rightarrow {}^7F_2(623\,\text{nm})$ transitions as a function of temperature are shown in Fig. 9(a). We can see that thermal quenching of both investigated transitions is very weak up to 330 K. For AlN doped with Tb^{3+} electric-dipole transitions originating from the $^5D_3$ or $^5D_4$ level exhibit well-separated groups of lines due to Stark splitting levels [Fig. 3(b)] and their inten-

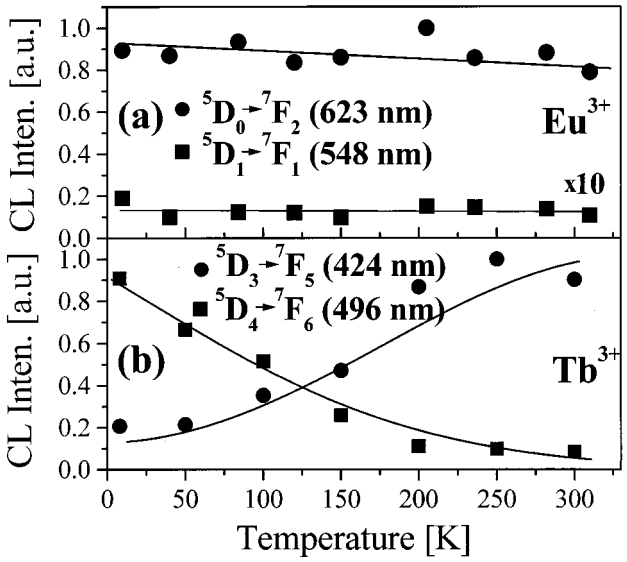

FIG. 9. Temperature dependence of CL intensity of selected Eu^{3+} (a) (●) and Tb^{3+} (b) (■) transition lines. Samples were excited by electron beam with energy 5 keV and current 1 mA/cm^2 and measured under identical excitation conditions. Solid lines are added as an aid to the eyes.

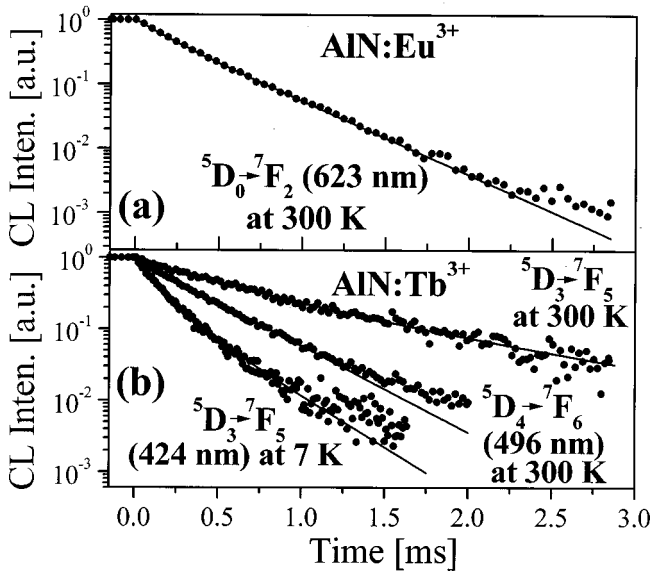

FIG. 10. The experimental CL decays of the strongest luminescent lines of Eu^{3+} (a) and Tb^{3+} (b) recorded at 7 and 300 K together with the fittings to expression including IH equation and extra exponential term (solid lines).

sities as a function of temperature are shown in Fig. 9(b). We found that transitions starting from these levels are very sensitive to ambient temperature and behave in the same manner when the temperature is changed. The energy gap between the $^5D_3$ and the $^5D_4$ states is about 5405 cm^{-1}. The AlN growth by different techniques shows oxygen and hydrogen contamination. The nonradiative relaxation from the $^5D_3$ state can be increased by the presence of OH groups due to their large vibrational frequency (3750 cm^{-1}) which significantly reduces the number of phonons necessary to cover the energy gap. Also, cross relaxation of $|^5D_3, ^7F_6\rangle \rightarrow |^5D_4, ^7F_{0,1}\rangle$ may contribute to these processes. Similar observations have been reported for amorphous Tb doped AlN film.[6] As mentioned above, the most probable location of RE ions in an AlN host is an Al site, and we can assume that there will be vibrational frequencies associated with localized motion of the impurity in addition to the band spectrum of the host lattice vibration. Since REs are heavier than the Al atom, a local vibration mode involving Eu or Tb will have a lower energy than the lattice modes, providing the force constants do not change greatly for this substitution. The most tightly bound centers are expected to have the strongest local-mode effect.[16] This may result in efficient energy transfer via multiphonon processes from the AlN host to the RE ion, which we believe is observed for the Tb doped AlN sample.

Furthermore, we studied CL kinetics for selected Eu^{3+} and Tb^{3+} ion transitions at different temperatures. The investigation of CL quenching of the singly doped (RE^{3+})AlN with temperature can provide information on interaction between like ions, ions with native defects, and ions with unintentionally incorporated impurities. At low doping concentrations of europium and terbium in AlN, the RE^{3+} ions form a disordered system with a wide range of inter-ion separations. For a resonant process an excitation can be transferred from the excited donor D^* to the neighboring donor ion in ground state (D) such that the second ion ends in the identical excited state D^*. We called that process a donor–donor ($D-D$) transfer.[17] This migration of the excitation over the donors changes the trapping efficiency since all excited donors, including those which are initially far away from any trap, can now transfer energy to donors which have traps as near neighbors. In order to determine the nature of the ion–ion interaction in this system we analyzed the decays of several emission lines of these ions as a function of temperature on the basis of the Inokuti–Hirayama (IH) model.[17] The CL decay kinetics of the Eu^{3+} $^5D_0 \rightarrow ^7F_2$ at 623 nm and Tb^{3+} $^5D_3 \rightarrow ^7F_5$ at 424 nm and $^5D_4 \rightarrow ^7F_6$ at 496 nm emissions have been measured at different temperatures and the experimental decay time data together with the fitting to expression including IH equation and exponential term are shown as semilog plots normalized to unity at $t=0$ in Fig. 10. The early part of the decay curves in Fig. 10 are nonexponential while the late-time luminescence decay is approximately exponential with radiative times, listed in Table II. This suggests that some of the Eu^{3+} and Tb^{3+} ions are in very isolated sites. The deviation from exponential data for the very-late part of the decay curves may be due to multisite phenomena or other processes like resonant and nonresonant energy transfer or upconversion not included here. The

TABLE II. Decay times of an exponential component in CL decay for selected transitions of Eu^{3+} and Tb^{3+} ions measured at 7 and 300 K.

	Eu^{3+}	Tb^{3+}	
	$^5D_0 \rightarrow ^7F_2$	$^5D_3 \rightarrow ^7F_5$	$^5D_4 \rightarrow ^7F_6$
	623 nm	424 nm	492 nm
		μs	
7 K	428.0	237.5	434.1
300 K	408.5	932.6	420.0

RE isoelectronic trap cannot necessarily be a pure substitutional center. Because the RE ions are very active chemically, they can create a more complex center involving other impurity or/and native defects.

IV. CONCLUSION

We have demonstrated that Eu^{3+} and Tb^{3+} ions implanted into AlN and annealed at 1100 °C in N_2 can be activated as efficient luminescence centers emitting in the UV and visible spectral regions under electron excitation. The characteristic RE intra-$4f^n$-shell transitions observed over the temperature range of 8–330 K are accompanied by much less intense host emission due to the oxygen presence and AlN structural defects. The CL kinetics was measured for $^5D_0 \rightarrow {}^7F_2(Eu^{3+})$, $^5D_3 \rightarrow {}^7F_5(Tb^{3+})$, and $^5D_4 \rightarrow {}^7F_6(Tb^{3+})$ transitions at 300 K and analyzed on the basis of IH model giving ~0.4, ~0.9, and ~0.4 ms decay times, respectively. Finally, the excitation mechanisms for RE^{3+} ions in the AlN host were discussed.

ACKNOWLEDGMENTS

H.J.L. and W.J. would like to acknowledge the support of the NSF through Grant No. ECS-0083412, BMDO Contract No. N00014-96-1-0782, and the O. U. Stocker Fund. The authors also gratefully acknowledge Raynald Gauvine for fruitful discussions.

[1] M. J. F. Digonnet, *Rare Earth Doped Fiber Lasers and Amplifiers* (Dekker, New York, 1993).
[2] A. Polman, J. Appl. Phys. **82**, 1 (1997).
[3] R. G. Wilson, R. N. Schwartz, C. R. Abernathy, S. J. Pearton, N. Newman, M. Rubin, T. Fu, and J. M. Zavada, Appl. Phys. Lett. **65**, 992 (1994).
[4] A. Young, S. Goss, L. Brillson, J. D. Mackenzie, and C. R. Abernathy, J. Electron. Mater. **29**, 311 (2000).
[5] K. Gurumurugan, H. Chen, G. R. Harp, W. M. Jadwisienczak, and H. J. Lozykowski, Appl. Phys. Lett. **74**, 3008 (1999).
[6] W. M. Jadwisienczak, H. J. Lozykowski, F. Perjeru, H. Chen, M. Kordesch, and I. Brown, Appl. Phys. Lett. **76**, 3376 (2000).
[7] H. J. Lozykowski, W. M. Jadwisienczak, J. Han, and I. G. Brown, Appl. Phys. Lett. **77**, 767 (2000).
[8] J. Reifsnider, D. Gotthold, A. Holmes, Jr., and B. Streetman, J. Vac. Sci. Technol. B **16**, 1278 (1998).
[9] (a) M. Morita, K. Tsubouchi, and N. Mikoshiba, Jpn. J. Appl. Phys., Part 1 **21**, 1102 (1982); (b) H. Markoc, *Nitride Semiconductors and Devices*, edited by R. Hull, R. M. Osgood, Jr., H. Sakaki, and A. Zunger (Springer, New York, 1999), p. 17; (c) A. Yoshida, *Properties, Processing and Applications of Galium Nitride and Related Semiconductors*, EMIS Data Reviews Series No. 23, edited by J. H. Edgar, S. Strirte, I. Akasaki, H. Amano, and C. Wetzel (London, 1999).
[10] G. H. Dieke, *Spectra and Energy Levels of Rare Earth Ions in Crystals* (McGraw–Hill, New York, 1968).
[11] (a) C. B. Norris, C. E. Barnes, and W. Beezhold, J. Appl. Phys. **44**, 3209 (1973); (b) K. Kanaya, and S. Okayama, J. Phys. D **5**, 43 (1972); (c) P. Hovington, D. Drouin, and R. Gauvin, Scanning **19**, 1 (1997); (d) **19**, 20 (1997); (e) **19**, 29 (1997).
[12] R. Shimizu, T. Ikuta, T. E. Everhart, and W. J. DeVore, J. Appl. Phys. **46**, 1581 (1975).
[13] C. Ronning, M. Dalmer, M. Uhrmacher, M. Restle, U. Vetter, L. Ziegeler, H. Hofsass, T. Gehrke, K. Jarrendahl, R. F. Davis, and ISOLDE Collaboration, J. Appl. Phys. **87**, 2149 (2000).
[14] H. J. Lozykowski, Phys. Rev. B **48**, 17758 (1993), and reference therein.
[15] J. B. Gruber, B. Zandi, H. J. Lozykowski, W. M. Jadwisienczak, and I. G. Brown, J. Appl. Phys. (in press).
[16] D. G. Thomas and J. J. Hopfield, Phys. Rev. **150**, 680 (1966).
[17] H. J. Lozykowski, W. M. Jadwisienczak, and I. Brown, J. Appl. Phys. **88**, 210 (2000), and reference therein.